Available online at www.sciencedirect.com
SCIENCE DIRECT®
Electrochimica Acta 49 (2004) 3373–3382
ELECTROCHIMICA Acta
www.elsevier.com/locate/electacta

In situ synchrotron X-ray studies on copper–nickel 5 V Mn oxide spinel cathodes for Li-ion batteries

S. Mukerjee [a], X.Q. Yang [b], X. Sun [b], S.J. Lee [b], J. McBreen [b], Y. Ein-Eli [c,*]

[a] *Chemistry Department, Northeastern University, Boston, MA 02115, USA*
[b] *Department of Applied Science, Brookhaven National Laboratory, Upton, NY 11973, USA*
[c] *Department of Materials Engineering, Technion-Israel Institute of Technology, Haifa 32000, Israel*

Received 12 August 2003; received in revised form 15 March 2004; accepted 15 March 2004

Available online 13 May 2004

Abstract

Partial substitution of Mn in lithium manganese oxide spinel materials by Cu and Ni greatly affects the electrochemistry and the cycle life characteristics of the cathode. Substitution with either metal or a combination of both metals in the spinel lattice structure reduces the 3.9–4.2 V potential plateaus associated with the conversion of Mn^{3+} to Mn^{4+}. Higher potential plateau associated with oxidation of the substituted transition elements is also observed. These substituents also significantly alter the onset of Jahn–Teller distortions in the 3 V potential plateau. Synchrotron based in situ X-ray absorption (XAS) was used to determine the exact nature of the oxidation state changes in order to explain the overall observed capacities at different potential plateaus. The studies on $LiCu_{0.5}Mn_{1.5}O_4$ show single phase behavior in the 4–5 V potential region with a good cycle life. Lower cycle life characteristic observed in cycling $LiNi_{0.5}Mn_{1.5}O_4$ and $LiNi_{0.25}Cu_{0.25}Mn_{1.5}O_4$ versus Li metal are ascribed to coexistence of several phases in this potential region. However, $LiCu_{0.5}Mn_{1.5}O_4$ shows onset of Jahn–Teller distortions in the 3 V potential plateau, in contrast to $LiNi_{0.5}Mn_{1.5}O_4$ and $LiNi_{0.25}Cu_{0.25}Mn_{1.5}O_4$ cathode materials.

Keywords: Synchrotron X-ray studies; Mn oxide spinel cathodes; Li-ion batteries; Copper–nickel 5 V cathode materials

1. Introduction

$LiMn_2O_4$ spinel materials are a very attractive choice as cathode material for lithium-ion rechargeable batteries due to their economical and environmental advantages over the current state of the art $LiCoO_2$. Previous reports by Tarascon et al. [1] and Thackarey and co-workers [2] demonstrated that addition of excess Li to the spinel ($Li_{1+x}Mn_{2-x}O_4$) improves the cathode cycle life, along with a concomitant decrease in the observed capacity. The capacity loss was reported to be $148(1-3x)$ mAh/gm [2]. Detailed analysis of this effect in the context of Li–Mn–O phase diagram related to $LiMn_2O_4$–$Li_4Mn_5O_{12}$–$Li_2Mn_4O_9$ cathode materials has been also reported by Xia et al. [3].

Another approach involves the substitution of a second transition element instead of Mn in the spinel oxide matrix, obtaining a general composition of $LiM_xMn_{2-x}O_4$. Attempts to substitute Mn with elements such as Co, Mg, Cr, Ni, Fe, Ti and Zn have been reported previously [4–6]. Initial results on these materials reported a lower capacity in the 4.1 V potential plateau compared with $LiMn_2O_4$ spinel [4–6]. However, a significant improvement in cycle life was reported with Ni, Co[6], and Cu substituted sample materials [7,8]. Later studies showed that some of these mixed oxide spinels possess a higher voltage plateau between 4.5 and 5.0 V, as was reported with Cu [7,8], Ni [9,10], Cr [11], Fe [11,12]. Sigala et al. [11] (based on electrochemical characterization), attributed the appearance of two voltage plateaus in Cr modified Mn spinel to the oxidation of Mn and Cr, respectively. Zhong et al. [9] reported that extraction of Li from Ni modified Mn spinel, $LiNi_xMn_{2-x}O_4$ (where $0 < x < 0.4$) provides an additional potential plateau at 4.6–4.7 V (in addition to the 4.1 V potential plateau). Only the higher potential plateau was obtained once x is equivalent to 0.5 in $LiNi_xMn_{2-x}O_4$, attributed to the oxidation of Ni^{2+} to Ni^{4+}. A simple model was proposed wherein, the oxidation state of the compound was expressed as

* Corresponding author. Tel.: +1-972-48294588; fax: +1-972-8295677.
E-mail addresses: s.mukerjee@neu.edu (S. Mukerjee), eineli@tx.technion.ac.il (Y. Ein-Eli).

0013-4686/$ – see front matter © 2004 Elsevier Ltd. All rights reserved.
doi:10.1016/j.electacta.2004.03.006

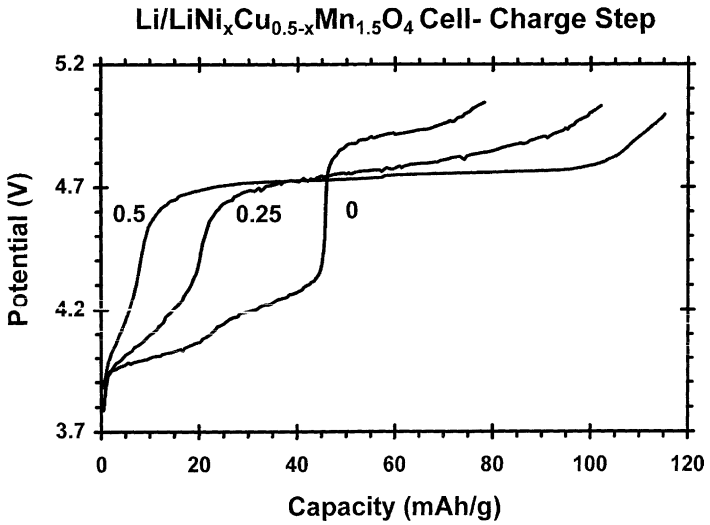

Fig. 1. Potential (V)-specific capacity (mAh/g) profiles obtained from $LiNi_xCu_{0.5-x}Mn_{1.5}O_4$ [$x = 0.0$, 0.25 and 0.5] during charge step in the 4–5 V region at 100 μA/cm^2.

$LiNi_x{}^{2+}Mn_{1-2x}{}^{3+}Mn_{1+x}{}^{4+}O_4{}^{2=}$, with the capacity in the lower plateau varying as $1-2x$Li/FU. Ohzuku et al. [12,13] produced a series of iron doped spinels ($LiFe_xMn_{2-x}O_4$) with a reversible capacity in the 5 V region. Recently, Fey et al. [14] prepared and evaluate high potential cathode materials based on $LiM_xNi_{0.5-x}Mn_{1.5}O_4$ (M being Fe, Cu, Al, and Mg while $0 < x < 0.4$). The authors found [14] that the best composition was the low doped iron ($x = 0.1$) nickel (0.4) Mn spinel.

This study involves the combination of in situ X-ray absorption and diffraction techniques aimed at investigating Cu and Ni substitutions in Mn oxide spinel cathodes with the general composition of $LiNi_xCu_{0.5-x}Mn_{1.5}O_4$, (where $x =$ 0, 0.25 and 0.5). The objective of this research was to rationalize the electrochemical characteristics of these spinels in the 4–5 V as well as the 3 V plateaus with direct spectroscopic measurements of changes in the oxidation states of the various transition elements. Synchrotron based in situ X-ray absorption spectroscopy allows such monitoring with element specificity along with determination of changes in the short range atomic order around the absorbing transition elements. Moreover, determining the nature of phase transitions at the different potential plateaus using in situ X-ray diffraction enables a better understanding of the spinel cathodes cycle life characteristics.

2. Experimental

Samples with general composition of $LiNi_xCu_{0.5-x}Mn_{1.5}O_4$ with $x = 0$, 0.25 and 0.5, were prepared using low temperature sol–gel techniques described in detail elsewhere [7,8,15]. Electrodes [with 5-6 mg/cm^2 loading of active material] were cast (doctor bladed) using a slurry comprising of 80% spinel Mn oxide, 10% carbon black (Shawinigan Acetylene black) and 10% polyvinylidene binder with 1-methyl-2-pyrrolidone as a solvent on an aluminum substrate (~5 μm thick), dried at 120 °C under vacuum for 2 h. Li metal served both as a counter and a reference electrode in the electrochemical cell. Details of the electrochemical tests are given in [7,8,15]. Cells were tested in the potential plateaus of 3.3–5.2 and 3.3–2.2 V separately. The electrolyte of choice in these tests were ethylene carbonate (EC, EM Industries) and ethyl methyl carbonate (EMC, Mitsubishi Chemicals) in a volume ratio of 1:3 with 1 M $LiPF_6$ salt.

Table 1
Electrochemical characteristics of $LiNi_xCu_{0.5-x}Mn_{1.5}O_4$ where $x = 0.0$, 0.25 and 0.50 in the 4–5 and 3 V regions

Cathode material	Potential (V) plateau's in the 4–5 V region		Discharge capacity (mAh/g)		Capacity in the 3 V region[a]	Capacity fade in 4–5 V region (%)[b]
			3.3–4.5 V	4.5–5.2 V		
$LiCu_{0.5}Mn_{1.5}O_4$	4.15	4.9	47	24	61	8
$LiCu_{0.25}Ni_{0.25}Mn_{1.5}O_4$	4.10	4.75	21	79	57	18
$LiNi_{0.5}Mn_{1.5}O_4$	4.10	4.6	12	105	54	12

[a] Capacity measured at the fifth cycle.
[b] Cycle life determined for a total of 50 cycles.

In situ XAS and XRD studies were performed with electrode loading of ∼20 mg/cm^2 active material with an electrode area of 2.85 cm^2. An electrochemical cell, designed for spectroscopic measurements in the transmission mode was used. Details of the spectro-electrochemical cell are given elsewhere [16]. In situ XAS measurements were conducted at Mn, Ni and Cu K edges at Beam line X11 A at the National Synchrotron Light Source, Brookhaven National Laboratory. The beam was detuned by 50% at the Mn K edge and 25% at the Ni and Cu K edges to reject higher harmonics. The spectra were collected up to the energy wave vector space of 18 K enabling simultaneous measurement of both XANES and EXAFS. Three detectors, incident, transmitted and references were used; the third detector serving as a reference for a proper alignment of the edge positions. XANES data was analyzed in detail since our primary interest was to determine the oxidation states of the Mn, Ni and Cu ions. The methods used for analyzing the XANES data are given in detail elsewhere [17]. The X-ray absorption spectra (XAS) collected with the storage ring operating at 2.584 GeV and an electron current between 110 and 350 mA. Details of the monochromator design, detune, data acquisition are given elsewhere [18]. Nominal energy resolution at 9 KeV (Cu K edge) was ∼1.1 eV for XANES and the relative position of the edges were measured with an accuracy of ±0.1 eV. As pointed out earlier [19], valence measured by XANES reflects the difference in energy of an initially unexcited atom in the solid and the same atoms with a core hole plus a photoelectron in the lowest energy unoccupied state of appropriate symmetry as determined by dipole selection rules. Oxidation state changes were based on standard curves obtained from shift in the XANES spectra at Mn, Cu and Ni K edge using standard compounds. Details of this measurements including shifts of XANES per oxidation state change are given elsewhere [8,15,16].

A series of standards for the determination of oxidation states using XANES at the Cu K edge were employed. These included Cu foil, Cu_2O, CuO and $KCuO_2$, in which Cu atoms assume monovalent, divalent and tetravalent states. As reported by us earlier [8], comparison of $LiMn_{1.5}Cu_{0.5}O_4$ (at open circuit, before charge or discharge) with standards clearly indicated that Cu is present only as Cu^{2+} with a symmetric coordination with planer and axially coordinated oxygen atoms. Detailed theoretical and experimental studies at the Cu K edge for a variety of standards including the ones used in the study has been conducted by Tranquada et al. [19]. As pointed out earlier by us [8], and others [20] the two prominent Cu edge XANES features representing an overlap of electric dipole transitions from 1s to various *n*p final states. The two main Cu XANES features which correspond to transitions from 1s to axially and planer 4p states typically show shifts of 2 eV per change in valence.

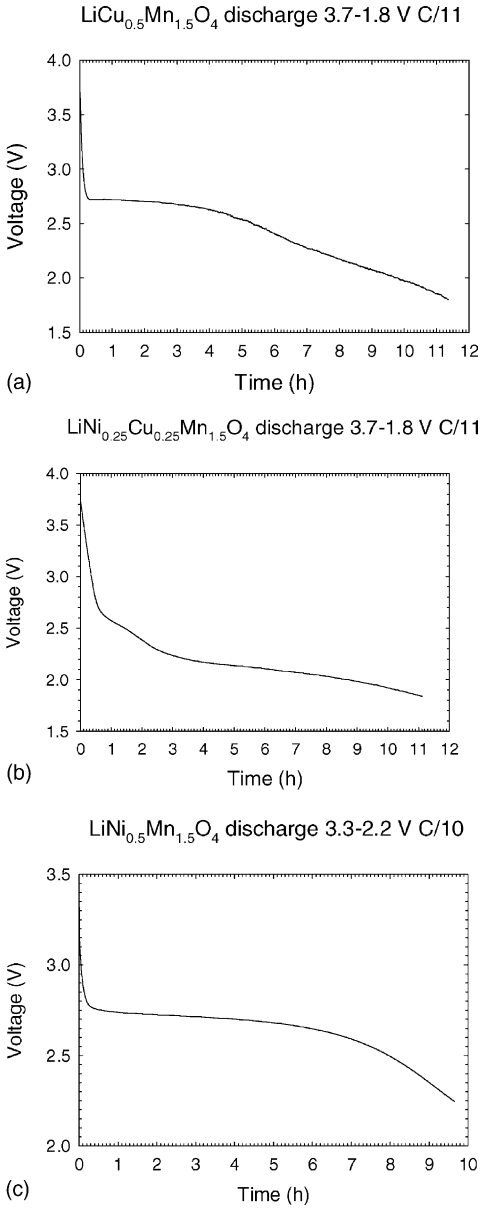

Fig. 2. Discharge profiles of $LiNi_xCu_{0.5-x}Mn_{1.5}O_4$: (a) $x = 0.0$; (b) $x = 0.25$; and (c) $x = 0.50$, in the 3 V region. Discharge was performed at ∼*C*/10 (100 μA/cm^2).

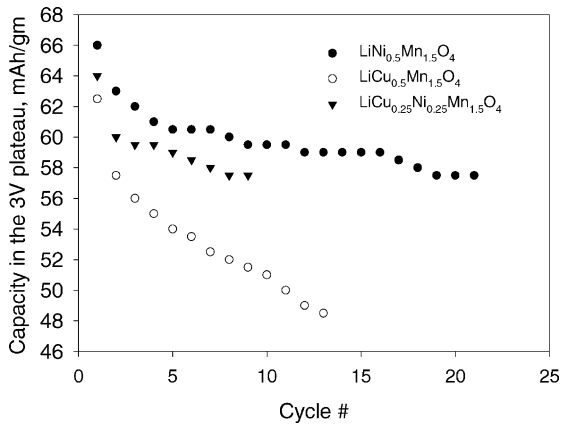

Fig. 3. Cycle life characteristics of $LiNi_xCu_{0.5-x}Mn_{1.5}O_4$ [$x = 0.0$, 0.25 and 0.50] in the 3 V region discharged at ∼*C*/10 (100 μA/cm^2).

The Mn oxidation states were measured with the use of several standards which included Mn, MnO, Mn_2O_3, MnO_2 (CMD, chemically prepared analog). Previously, we have reported that XANES data for the CMD and EMD (electrochemically prepared analog) of MnO_2 were identical. In addition, a comparison with $LiMn_{1.5}Cu_{0.5}O_4$ (at open circuit, before charge or discharge), showed a shoulder at 11.5 eV, consistent with the presence of both Mn^{4+} and a very small amount of Mn^{3+}. Details of the shifts per change in valence state and the assignment of Mn features in the Mn edge XANES is provided in detail elsewhere [21,22]. Similarly, Ni oxidation states were analyzed with the use of freshly prepared Ni, α-$Ni(OH)_2$, α-NiOOH and $BaNiO_3$, compounds. The two distinct features in the Ni edge XANES have been carefully analyzed in terms of shifts as a function of change in the Ni valence states [18,23–26].

Samples studied by XAS and XRD in the 4–5 V region were conducted at charging/discharging rate of *C*/12. Samples investigated at the 3 V region were studied at a rate of *C*/10. XANES spectra were taken for the second charge and discharge cycle. Since the data at the Cu, Ni and Mn edges were taken from the same cell during the charge and discharge process, the procedure adopted involved interrupting the charge/discharge process and allowing the cell to reach equilibrium (this was achieved by monitoring the potential profiles at open circuit). Data was then collected serially at the Cu, Ni and Mn edges. Thus, the number of data points for oxidation states were limited. In situ XRD measurements were conducted at Beam line X18 A in the

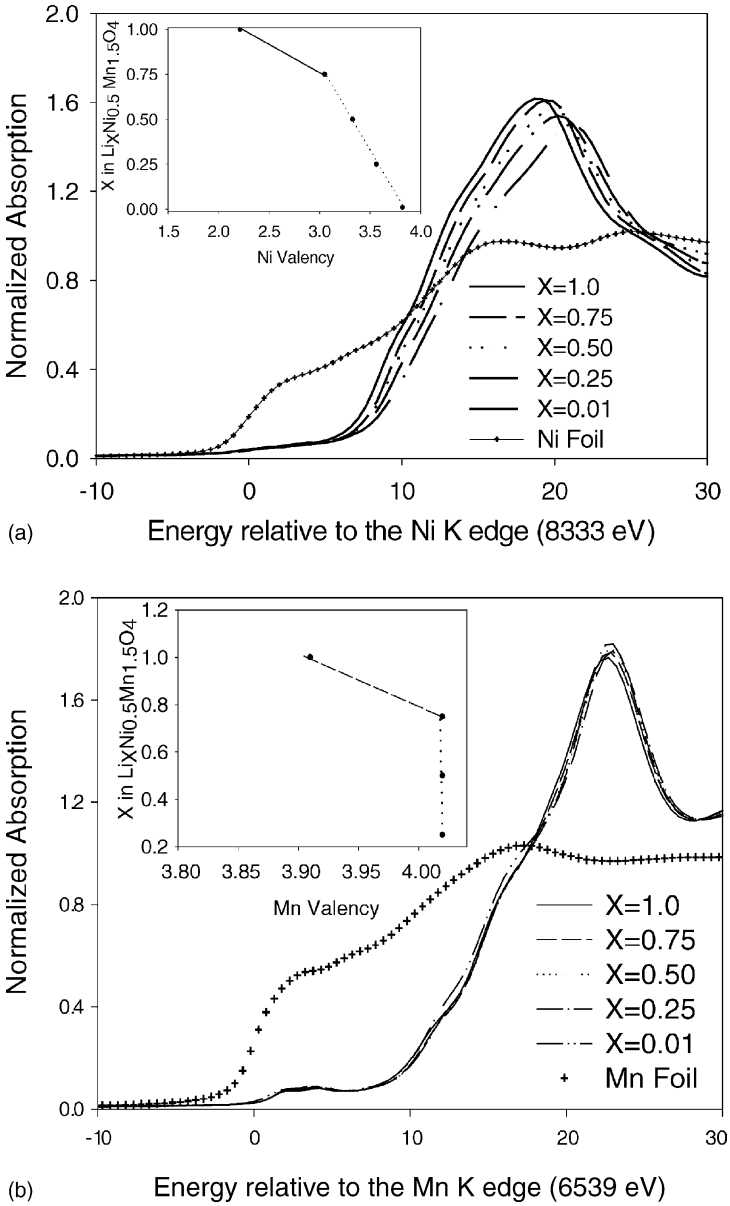

Fig. 4. XANES at: (a) Ni; and (b) Mn K edge for $LiNi_{0.5}Mn_{1.5}O_4$ as a function of charge (*C*/12 rate) in the 4–5 V region. Inset in the figure show the corresponding changes in the Ni and Mn oxidation states.

transmission mode with monochromatic beam tuned to a wavelength λ of 1.195 Å corresponding to 10.375 KeV. Advantages of synchrotron based XRD are outlined in detail elsewhere [27,28]. Successive scans between 2θ angles of 43 and 53° were used to monitor the coinciding peaks ⟨3 3 1⟩, ⟨5 1 1⟩ as well as the ⟨4 4 0⟩ and ⟨5 3 1⟩ peaks of the spinel. The aluminum substrate ⟨2 2 0⟩ peak served as an internal standard.

3. Results and discussion

3.1. Electrochemical characterization

Figs. 1 and 2 presents the potential profiles obtained from polarizing $LiNi_xCu_{0.5-x}Mn_{1.5}O_4$ (where $x = 0$, 0.25 and 0.5) versus Li metal in the 4–5 and 3 V regions. Table 1 summarizes the discharge capacity values obtained as a function of the corresponding oxide compositions. Several observations can be made:

(i) The inclusion of Ni in $LiNi_xCu_{0.5-x}Mn_{1.5}O_4$ spinels reduces the potential at the high potential region. The upper potential plateau observed in polarizing $LiCu_{0.5}Mn_{1.5}O_4$ was 4.9 V, while substituting half of the copper with nickel, producing $LiCu_{0.25}Ni_{0.25}Mn_{1.5}O_4$, reduced the upper potential plateau by 150 mV to 4.65 V, as can be observed in Fig. 1. The potential plateau is further reduced by another 150 mV to the potential of 4.6 V once a complete substitution of copper with nickel [$LiCu_{0.5}Mn_{1.5}O_4$] in the spinel matrix takes place.

(ii) Increasing the Ni content in the spinel structure reduces the capacity of the medium potential plateau (3.3–4.5 V) and increases the capacity of the high voltage plateau (4.5–5.2 V). However, the capacity value obtained from the lower voltage plateau region, which is attributed to the reversible transition of Mn^{3+} to Mn^{4+}, is not totally eliminated. The electrochemical results obtained from the spinel electrode with the composition of $LiNi_{0.5}Mn_{1.5}O_4$ show that not all the Mn is tetravalent as expected from charge neutrality considerations and from those based on simplistic models of Amine et al. [10] and Gao et al. [29].

(iii) As x in $LiNi_xCu_{0.5-x}Mn_{1.5}O_4$ increases (Table 1), the capacity value at the medium potential region (3.3–4.5 V) reduces from 47 mAh/g [in $LiCu_{0.5}Mn_{1.5}O_4$ ($x = 0$)] to 12 mAh/g [in $LiNi_{0.5}Mn_{1.5}O_4$ ($x = 0.5$)]. Conversely, the capacity value obtained at the high voltage plateau (4.5–5.2 V) increased from 24 mAh/g [in $LiCu_{0.5}Mn_{1.5}O_4$ ($x = 0$)], to 79 mAh/g [in $LiCu_{0.25}Ni_{0.25}Mn_{1.5}O_4$ ($x = 0.25$)] to 105 mAh/g [in $LiNi_{0.5}Mn_{1.5}O_4$ ($x = 0.5$)].

(iv) The overall capacity value in the 4–5 V range obtained from the Ni rich sample is higher, compared with the Cu rich oxide samples. This can be attributed to a two electron transfer in Ni (Ni^{2+} to Ni^{4+}) and the possibility of Ni occupying B sites in the spinel octahedra in a higher concentration as compared to Cu.

(v) The capacity values in the low 3 V plateau shows comparable performance for all three materials (Fig. 3), indicating that the capacity origin is due to the reduction of Mn^{4+} to Mn^{3+}. However, the discharge profile is different for each composition: the Ni rich composition (Fig. 2c) possess the highest discharge capacity and has a wide range potential plateau at 2.8 V with

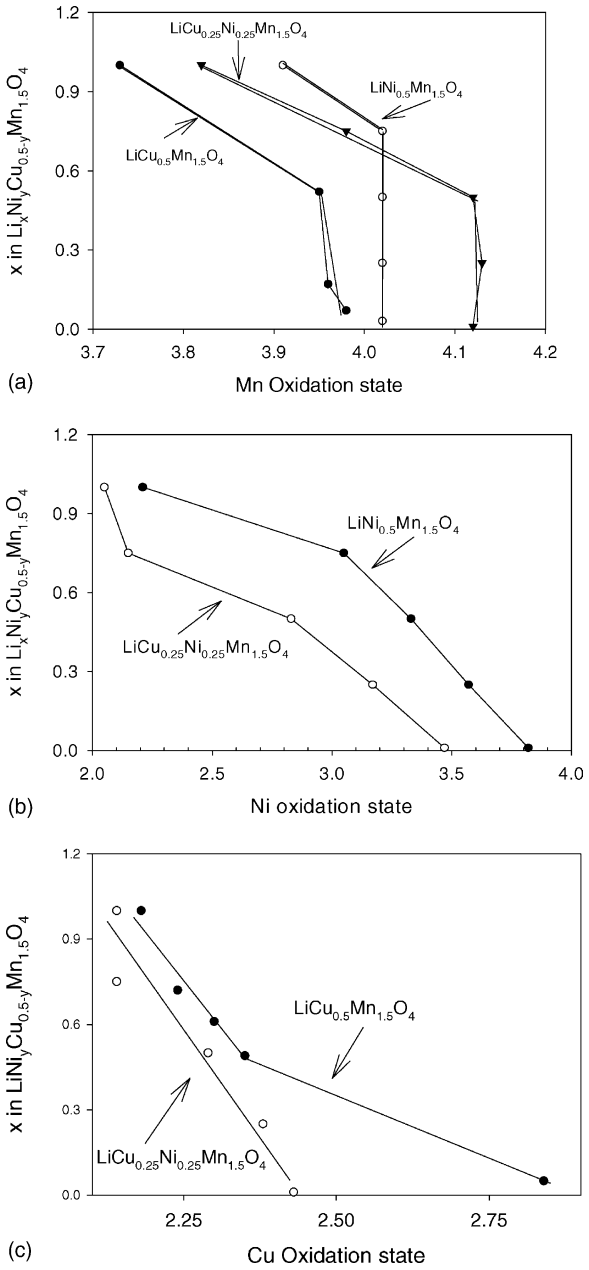

Fig. 5. Summary of oxidation state changes for: (a) Mn; (b) Ni; and (c) Cu in $LiNi_xCu_{0.5-x}Mn_{1.5}O_4$ [$x = 0.0$, 0.25 and 0.50], determined from XANES analysis of the corresponding Mn, Ni and Cu K edge spectra as a function of charge in the 4–5 V region. Cycle rate for each sample was kept constant at $C/12$.

a moderate decrease in the potential after 70% discharge time (approximately 45 mAh/g). In contrast to this behavior, the copper rich spinel matrix presents a totally different profile; we initially observe in two potentials regions. The first one is a potential plateau at 2.75 V (first 6 h, 30 mAh/g) which transformed into a slope one. The total capacity recorded for this cathode matrix was measured to be also the lowest one, 57 mAh/g. The blend Ni/Cu cathode matrix presents an intermediate behavior (overall capacity of less than 55 mAh/g) with two distinguished potential plateaus: the first one is observed at 2.6 V with a small capacity of ∼15 mAh/g while the second potential plateau at 2.3 V is the longest one (40 mAh/g).

Finally, the cycle life performance shows that in the 4–5 V region, the Cu substituted sample has the highest stability despite the higher voltage range. Increased Ni substitution results in steady decay of the life time stability (Table 1). However, in the 3 V region (Fig. 3), the situation is reversed;

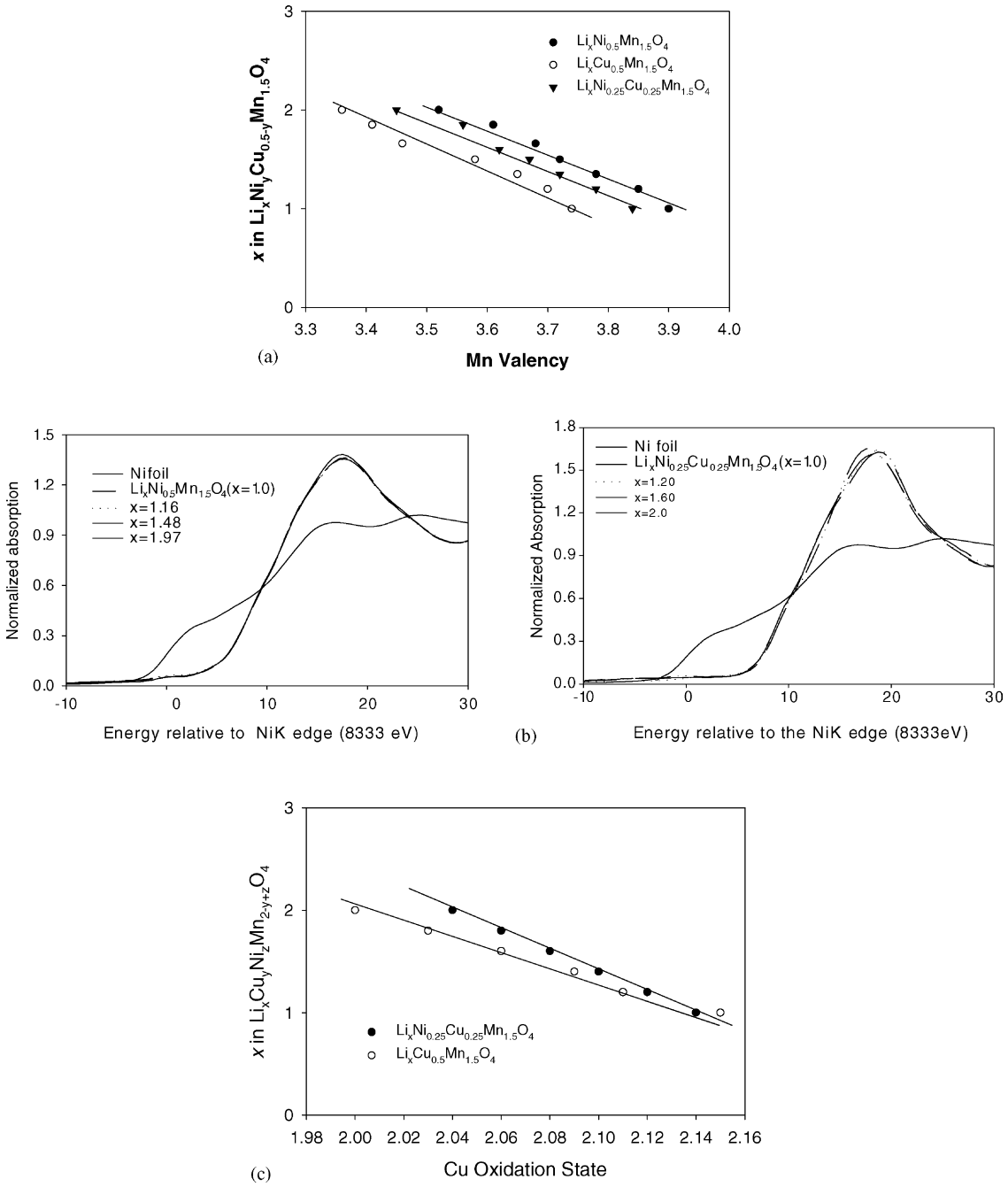

Fig. 6. The effect of Li intercalation in the 3 V region on: (a) Mn; (b) Ni; and (c) Cu oxidation states in $LiNi_xCu_{0.5-x}Mn_{1.5}O_4$ [$x = 0.0$, 0.25 and 0.50] determined from XANES analysis of the corresponding Mn, Ni and Cu K edge spectra. Discharge rate was *C*/10.

the Cu substituted spinel sample shows the worst performance and increased Ni substitution caused significant improvement in the cycle life of the spinel electrode.

3.2. In situ XAS studies

Fig. 4a and b show representative plots of Ni and Mn K edge XANES spectra obtained from $LiNi_{0.5}Mn_{1.5}O_4$ as a function of charge in the 4–5 V region. Both Ni and Mn edge shifts are observed, indicating changes in their respective oxidation states. In agreement with previous work by Amine et al. [10], who examined the lower voltage plateau (3.3–4.5 V), there is a little evidence for the existence of Mn^{3+} state; the starting oxidation state in the material is 3.9 (inset in Fig. 4b). Upon charging, Mn oxidation state changes rapidly in the small residual low voltage plateau (Fig. 1) to +4. In the higher voltage plateau there is no change in this oxidation state, in agreement with our previous results [15,16]. Ni K edge XANES indicates that most of the capacity is originated from a change in Ni oxidation state. This corresponds to a voltage plateau of 4.6 V (Fig. 1). While Mn oxidation state was minored changed (oxidation state change of only 0.1 was observed), Ni oxidation state change corresponds to 1.6 (from 2.2 to 3.8) (inset in Fig. 4a). The modifications in the oxidation states correspond well with the observed capacities in the low and high voltage plateaus (Table 1).

Fig. 5, shows a compilation of oxidation state changes in Mn, Ni and Cu for $LiNi_xCu_{0.5-x}Mn_{1.5}O_4$ (for $x = 0.0$, 0.25, and 0.5) using similar XANES analysis. The changes in the oxidation states are in a good agreement with the electrochemical results presented in Table 1 and Fig. 1. The two plateaus at 3.3–4.1 and 4.1–5.2 V observed in $LiCu_{0.5}Mn_{1.5}O_4$ correspond to changes in Mn and Cu oxidation states in the range 3.7–4.0 and 2.18–2.84 V, respectively. Considering the results obtained from the

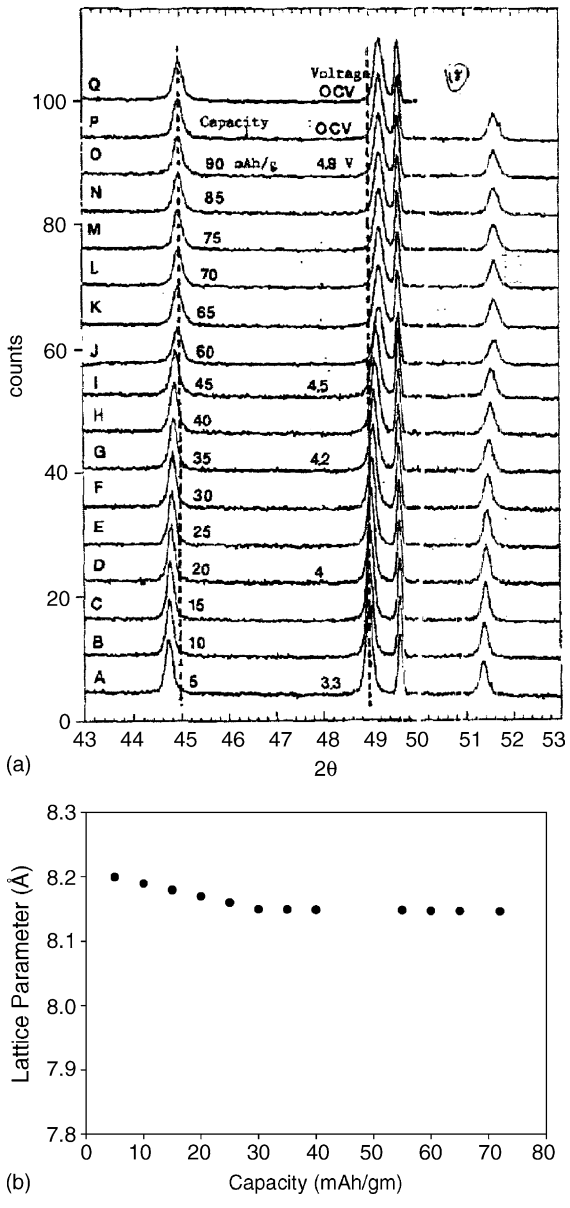

Fig. 7. In situ XRD patterns for $LiCu_{0.5}Mn_{1.5}O_4$ during second charge cycle in the 4–5 V region: (a) change in the XRD profile in the 2θ range of 43–53° for a λ value of 1.195 Å; and (b) the corresponding lattice parameters vs. capacity plot: (●) first cubic phase. Sample was charged at *C*/12 rate.

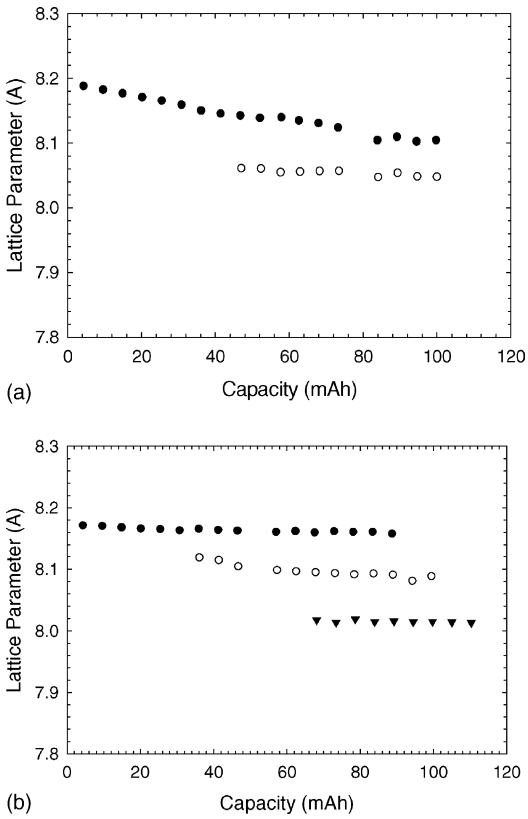

Fig. 8. Results of in situ XRD analysis for: (a) $LiNi_{0.25}Cu_{0.25}Mn_{1.5}O_4$; and (b) $LiNi_{0.5}Mn_{1.5}O_4$ during the second charge in the 4–5 V region. (●) First cubic phase; (○) second cubic phase; (▼) third cubic phase. Discharge rate was *C*/12.

composition of $LiCu_{0.25}Ni_{0.25}Mn_{1.5}O_4$ one would observe that in the low potential plateau the Mn oxidation state changes from 3.8 to 4.0, while at the higher potential plateau both Ni and Cu oxidation state are changed from 1.98 to 3.47 and 2.14 to 2.43 V, respectively.

Fig. 6 shows a similar compilation of oxidation state modifications in the 3 V region (3.3–2.2 V). As evident, the capacity in this region is originated due to a reduction of the Mn from Mn^{4+} to Mn^{3+} (Fig. 6a). The capacity values shown in Table 1 associated with this region show similar magnitudes and reflect this behavior. The Mn oxidation state changes in this region correspond to 3.75–3.35 for $LiCu_{0.5}Mn_{1.5}O_4$, while for $LiNi_{0.5}Mn_{1.5}O_4$ and $LiCu_{0.25}Ni_{0.25}Mn_{1.5}O_4$ these changes are in the ranges 3.9–3.45 and 3.85–3.45 V, respectively. The modifications in the oxidation state point that the oxidation state of Mn in Cu substitution spinel, $LiCu_{0.5}Mn_{1.5}O_4$, approaches closest to the Jahn–Teller Mn^{3+} high spin state ($3d^4$, $t_{2g}^3 e_g^1$), while for the other two compositions it lies close to an average oxidation state of $Mn^{3.45}$. This may explain the poor cycle life behavior obtained from this material at this potential region. Fig. 6b presents the changes in Ni oxidation state in both $LiNi_{0.5}Mn_{1.5}O_4$ and $LiNi_{0.25}Cu_{0.25}Mn_{1.5}O_4$. As evident, there are no changes in Ni oxidation states in this potential region. Fig. 6c shows the corresponding changes in Cu oxidation states for both $LiCu_{0.5}Mn_{1.5}O_4$ and $LiNi_{0.25}Cu_{0.25}Mn_{1.5}O_4$, which also exhibits minimal changes.

3.3. In situ XRD studies

In situ XRD (transmission mode) was used to monitor changes in the spinel cubic phase as a function of charge capacity in all three compositions. Second charge profile was studied in order to avoid problems associated with the initial charge–discharge cycle, such as surface passivation effects. Fig. 7a presents in situ XRD profiles of 2θ region, between 43 and 53°, corresponding to overlapping spinel peaks $\langle 3\,3\,1\rangle$, $\langle 5\,1\,1\rangle$ in addition to $\langle 4\,4\,0\rangle$ and $\langle 5\,3\,1\rangle$ peaks for $LiCu_{0.5}Mn_{1.5}O_4$ in the 4–5 V region. In contrast to the XRD profile of $LiMn_2O_4$ spinel material previously reported [27,28], there is a smooth transition at the end of the charge step as a single phase without the appearance of any additional phases. The diffraction peaks shift to a higher angle indicating a contraction of the lattice on removal of Li ions in the lower plateau (3.3–4.5 V), while at the higher potential plateau (4.5–5.2 V) no further contraction in the lattice is observed (Fig. 7b). Moreover, there is no evidence of any peak splitting which would have been indicative of two-phase coexistence. In situ XRD patterns obtained during discharge [8,15] demonstrate the reversibility of this single-phase behavior.

In a contrast, in situ XRD profiles obtained from $LiNi_{0.5}Mn_{1.5}O_4$ and $LiCu_{0.25}Ni_{0.25}Mn_{1.5}O_4$ (Fig. 8) show three and two phases coexistence in the upper voltage plateau (4.5–5.2 V). The patterns also indicate minimal changes in the lattice parameters within each phase. However, the

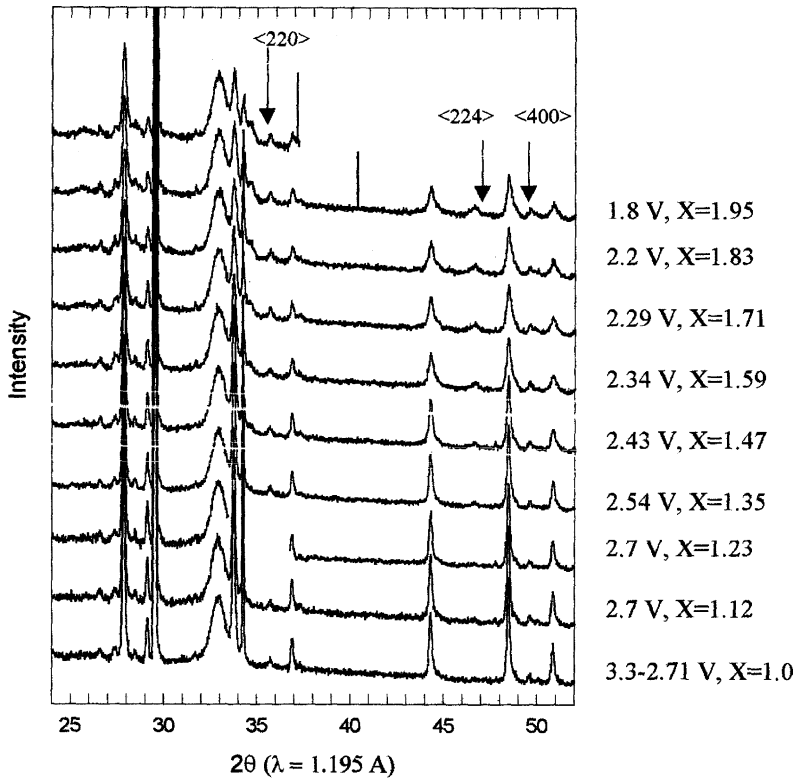

Fig. 9. In situ XRD pattern for a fresh $LiCu_{0.5}Mn_{1.5}O_4$ during Li intercalation in the 3 V region. The onset of tetragonal peaks marks the onset of Jahn–Teller distortions in this potential region. Discharge rate was *C*/10.

coexistence of several phases could be detrimental to the long term structural integrity of the lattice. This evidence can provide the explanation for the poor cycle life of these compositions in the 4–5 V region. The exact implications of the coexistence of several phase, its reversibility and implications to long term stability of the lattice will be the subject of a more detailed publication.

In situ XRD profiles in the 3 V region obtained from all material compositions ($LiCu_{0.5}Mn_{1.5}O_4$, $LiNi_{0.5}Mn_{1.5}O_4$ and $LiCu_{0.25}Ni_{0.25}Mn_{1.5}O_4$) are shown in Figs. 9–11. The profiles were obtained from a "fresh" cell during additional Li ion intercalation process. As evident from these profiles, $LiCu_{0.5}Mn_{1.5}O_4$ composition clearly shows the onset of the Jahn–Teller distortions (Fig. 9). The distortion is observed as early as x in $Li_xCu_{0.5}Mn_{1.5}O_4$ reaches a value of 1.12, corresponding to a potential of 2.7 V (or an equivalent) capacity of 10 mAh/gm. This is evident from the appearance of tetragonal peaks at ⟨2 2 0⟩, ⟨2 2 4⟩ and ⟨4 0 0⟩ in the 2θ range 23–53°. In a contrast, $LiNi_{0.5}Mn_{1.5}O_4$ and $LiCu_{0.25}Ni_{0.25}Mn_{1.5}O_4$ do not exhibit any Jahn–Teller distortion as evident from the absence of any tetragonal peaks (Figs. 10 and 11).

The absences of these peaks in both materials XRD's patterns indicate the high stability of Ni doped Mn spinel at low potentials (below 3 V) during charging excess of Li ion into the spinel matrix. This study confirms earlier observation based on changes in the oxidation states of $LiCu_{0.5}Mn_{1.5}O_4$ as compared with $LiNi_{0.5}Mn_{1.5}O_4$ and $LiCu_{0.25}Ni_{0.25}Mn_{1.5}O_4$ in this potential region. Therefore, the cycle life characteristics observed in Fig. 2 are in agreement with the results obtained from in situ XRD studies. While Cu substituted sample has the highest stability (despite the higher voltage range) leading to a long cycle life performance in the 4–5 V region, it shows the worst performance in the 3 V region. Increased Ni substitution caused a significant improvement in the cycle life of the modified Mn spinel electrode. Thus, the most stable compound at the 5 V region (Cu doped Mn spinel) has the worst performance at the 3 V region, while the best materials performed at this potential are the Ni doped Mn spinels. These compounds do not show a stable cycle life at the elevated potential. This behavior is linked to the phase transformation observed with the use of in situ XRD in our studies.

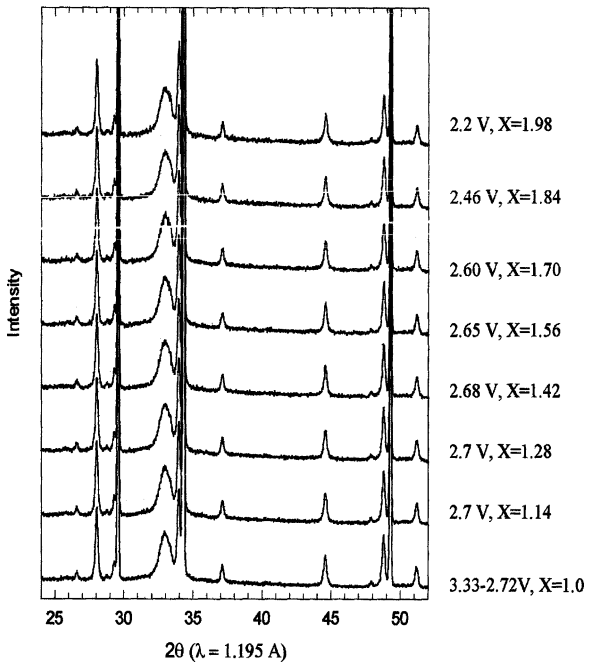

Fig. 10. In situ XRD pattern obtained from a fresh $LiNi_{0.5}Mn_{1.5}O_4$ during first Li-ion intercalation step at the 3 V region. Note the absence of tetragonal peaks indicating no Jahn–Teller distortions in this potential region. Discharge rate was *C*/10.

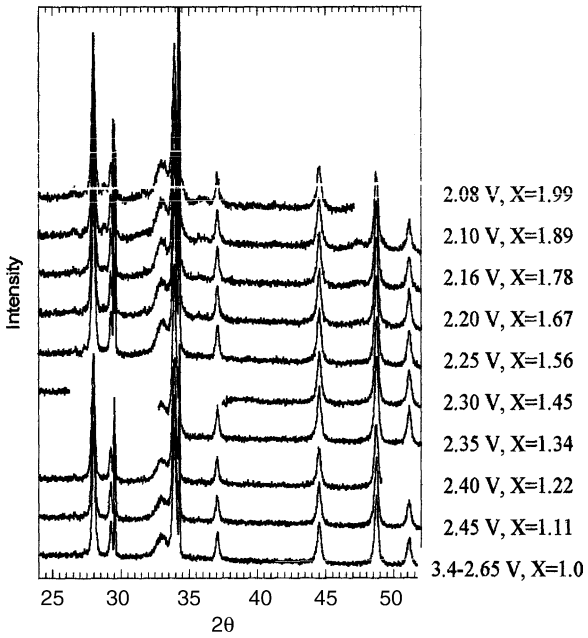

Fig. 11. In situ XRD pattern from a fresh $LiCu_{0.25}Ni_{0.25}Mn_{1.5}O_4$ during first Li intercalation step in the 3 V region. Note the absence of tetragonal peaks indicating no Jahn–Teller distortions in this potential region. Discharge rate was *C*/10.

4. Conclusions

$LiNi_xCu_{0.5-x}Mn_{1.5}O_4$ materials have been prepared and evaluated both electrochemically as well as using synchrotron based in situ XAS and XRD spectroscopy. The data show that Li can be extracted from the spinel structures in two main potential regions: 3.3–4.5 and 4.6–5.1 V. The upper potential is dependent on the value of x; as Ni content increases, the potential plateau decreases from 4.95 to 4.6 V. At the same time, the reversible capacity increases from approximately 72 mAh/g ($x = 0$) to 120 mAh/g ($x = 0.5$). In situ XAS spectroscopy shows that for a Cu rich composition ($x = 0$), the two potential plateaus correspond to a change in Mn oxidation state from 3.7 to 4.0 and a change in Cu oxidation state from 2.18 to 2.84. The change in Mn oxidation state in $LiCu_{0.25}Ni_{0.25}Mn_{1.5}O_4$ ($x = 0.25$) is

lower (from 3.8 to 4.0). Thus, most of the recorded capacity is a result of changes in the Ni oxidation state (from 1.98 to 3.47) and to a lesser extent a modification in Cu oxidation state (from 2.14 to 2.43). At $x = 0.5$ [$LiNi_{0.5}Mn_{1.5}O_4$] the measured capacity is originated from change in the Ni oxidation state (from 2.2 to 3.8). In the 3 V region, intercalation of Li results primarily in changes of Mn oxidation state. In Cu rich sample ($x = 0$), the Mn oxidation state approaches a value of 3.35, causing the onset of cooperative Jahn–Teller distortion. In contrast, the transition in the oxidation state observed for Mn in both compositions containing $x = 0.25$ and 0.0 [$LiCu_{0.25}Ni_{0.25}Mn_{1.5}O_4$ and $LiCu_{0.5}Mn_{1.5}O_4$, respectively] is to an oxidation state of 3.45. In situ XRD profiles in the 4–5 V region shows that Cu rich sample ($LiCu_{0.5}Mn_{1.5}O_4$, $x = 0.0$) has a single phase transition during charge and discharge. This is in contrast to two and three phases coexisting in compositions containing $x = 0.25$ and 0.5 [$LiCu_{0.25}Ni_{0.25}Mn_{1.5}O_4$ and $LiNi_{0.5}Mn_{1.5}O_4$, respectively]. This explains the superior cycle life behavior of Cu rich sample ($x = 0$) in the ultra-high potential region. In contrast to this unique behavior, Cu rich sample shows the onset of Jahn–Teller distortions in the 3 V region. Such distortions are absent in the Ni substituted materials ($x = 0.25$ and 0.5).

Acknowledgements

This work was supported by the Assistant Secretary for Energy Efficiency and Renewable Energy, Office of Transportation Technologies, Electric and Hybrid Propulsion Division, USDOE under Contract number DE-AC02-98CH10886 and by the Technion-Israel Institute of Technology.

References

[1] J.M. Tarascon, F. Coowar, G. Amatuci, F.K. Shokoohi, D.G. Guyomard, J. Power Sources 54 (1) (1995) 103–108.
[2] R.J. Gummow, A. de Kock, M.M. Thackeray, Solid State Ion. 69 (1994) 59.
[3] Y. Xia, M. Yoshio, J. Electrochem. Soc. 144 (1997) 4186.
[4] J.M. Tarascon, E. Wang, F.K. Shokoohi, W.R. McKinnon, S. Colson, J. Electrochem. Soc. 138 (1991) 2859.
[5] R. Bittihn, R. Herr, D. Hoge, J. Power Sources 44 (1993) 409.
[6] L. Guahua, H. Ikuta, T. Uchida, M. Wakihara, J. Electrochem. Soc. 143 (1996) 178.
[7] Y. Ein-Eli, W.F. Howard Jr., J. Electrochem. Soc. 144 (1997) L205.
[8] Y. Ein-Eli, W.F. Howard Jr., S.H. Lu, S. Mukerjee, J. McBreen, J.T. Vaughey, M.M. Thackeray, J. Electrochem. Soc. 145 (1998) 1238.
[9] Q. Zhong, A. Banakdarpour, M. Zhang, Y. Gao, J.R. Dahn, J. Electrochem. Soc. 144 (1997) 205.
[10] K. Amine, H. Tukamoto, H. Yasuda, Y. Fujita, J. Electrochem. Soc. 143 (1996) 1607.
[11] C. Sigala, D. Guyomard, A. Verbaere, Y. Piffard, M. Tournoux, Solid State Ion. 81 (1995) 167.
[12] T. Ohzuku, S. Takeda, M. Iwanaga, J. Power Sources 81–82 (1999) 90.
[13] T. Ohzuku, K. Ariyoshi, S. Takeda, Y. Sakai, Electrochim. Acta 46 (2001) 2327.
[14] G.T.-K. Fey, C.-Z. Lu, T.P. Kumar, J. Power Sources 115 (2003) 332.
[15] Y. Ein-Eli, J.T. Vaughey, M.M. Thackeray, S. Mukerjee, X.Q. Yang, J. McBreen, J. Electrochem. Soc. 146 (1999) 908.
[16] J. McBreen, S. Mukerjee, S. Srinivasan (Eds.), Proceedings of a Symposium on Electrode Materials and Processes for Energy Conversion and Storage IV, 4–9 May 1997, Montreal, Que., Canada (Proc. Electrochem. Soc. (1997) 97–13).
[17] J. Wong, F.W. Lytle, R.P. Messmer, D.H. Maylotte, Phys. Rev. B: Condens. Mat. Mater. Phys. 30 (1984) 5596.
[18] K.I. Pandya, R.W. Hoffman, J. McBreen, W.E. O'Grady, J. Electrochem. Soc. 137 (1990) 383.
[19] J.M. Tranquada, S.M. Heald, A.R. Moodenbaugh, Phys. Rev. B: Condens. Mat. Mater. Phys. 36 (1987) 5263.
[20] E.E. Alp, G.K. Shenoy, D.G. Hinks, D.W. Capone Jr., L. Soderholm, H.B. Schuttler, J. Guo, D.E. Ellis, P.A. Montano, M. Ramanathan, Phys. Rev. B: Condens. Mat. Mater. Phys. 35 (1987) 7199.
[21] B.H. Kim, J.S. Kim, D.C. Kim, Y.W. Park, A. Maignan, B. Raveau, Int. J. Modern Phys. B: Condens. Mat. Phys. Statist. Phys. Appl. Phys. 17 (2003) 3745.
[22] B. Ammundsen, D.J. Jones, J. Roziere, J. Solid State Chem. 141 (1998) 294.
[23] X. Qian, H. Sambe, D.E. Ramaker, K.I. Pandya, W.E. O'Grady, J. Phys. Chem. B 101 (1997) 9441.
[24] W.E. O'Grady, K.I. Pandya, K.E. Swider, D.A. Corrig, J. Electrochem. Soc. 143 (1996) 1613.
[25] K.I. Pandya, W.E. O'Grady, D.A. Corrigan, J. McBreen, R.W. Hoffman, J. Phys. Chem. 94 (1990) 21.
[26] J. McBreen, W.E. O'Grady, G. Tourillon, E. Dartyge, A. Fontaine, K.I. Pandya, J. Phys. Chem. 93 (1989) 6308.
[27] S. Mukerjee, T.R. Thurston, N.M. Jisrawi, X.Q. Yang, J. McBreen, M.L. Daroux, X.K. Xing, J. Electrochem. Soc. 145 (1998) 466.
[28] X.Q. Yang, X. Sun, S.J. Lee, J. McBreen, S. Mukerjee, M.L. Daroux, X.K. Xing, Electrochem. Solid-State Lett. 2 (1999) 157.
[29] Y. Gao, K. Myrtle, M. Zhang, J.N. Reimers, J.R. Dahn, Phys. Rev. B: Condens. Mat. 54 (1996) 16670.